Am J Physiol Cell Physiol 297: C1091–C1102, 2009.
First published August 19, 2009; doi:10.1152/ajpcell.00177.2009.

Bicarbonate homeostasis in excitable tissues: role of AE3 Cl^-/HCO_3^- exchanger and carbonic anhydrase XIV interaction

Joseph R. Casey,[1] William S. Sly,[2] Gul N. Shah,[2] and Bernardo V. Alvarez[3]

[1]*Department of Physiology and Department of Biochemistry, Membrane Protein Research Group, University of Alberta, Edmonton, Canada;* [2]*Department of Biochemistry and Molecular Biology, Saint Louis University School of Medicine, St. Louis, Missouri; and* [3]*Centro de Investigaciones Cardiovasculares, Facultad de Ciencias Médicas, Universidad Nacional de La Plata, La Plata, Argentina*

Submitted 24 April 2009; accepted in final form 16 August 2009

Casey JR, Sly WS, Shah GN, Alvarez BV. Bicarbonate homeostasis in excitable tissues: role of AE3 Cl^-/HCO_3^- exchanger and carbonic anhydrase XIV interaction. *Am J Physiol Cell Physiol* 297: C1091–C1102, 2009. First published August 19, 2009; doi:10.1152/ajpcell.00177.2009.—Bicarbonate transport and metabolism are key elements of normal cellular function. Two alternate transcripts of anion exchanger 3 (AE3), full-length (AE3fl) and cardiac (AE3c), are expressed in central nervous system (CNS), where AE3 catalyzes electroneutral Cl^-/HCO_3^- exchange across the plasma membrane of neuronal and glial cells of CNS. Anion exchanger isoforms, AE3fl and AE3c, associate with the carbonic anhydrases (CA) CAII and CAIV, forming a HCO_3^- transport metabolon, to maximize HCO_3^- flux across the plasma membrane. CAXIV, with catalytic domain anchored to the extracellular surface, is also expressed in CNS. Here physical association of AE3 and CAXIV was examined by coimmunoprecipitation experiments, using mouse brain and retinal lysates. CAXIV immunoprecipitated with anti-AE3 antibody, and both AE3 isoforms were immunoprecipitated using anti-CAXIV antibody, indicating CAXIV and AE3 interaction in the CNS. Confocal images revealed colocalization of CAXIV and AE3 in Müller and horizontal cells, in the mouse retina. Cl^-/HCO_3^- exchange activity of AE3fl was investigated in transiently transfected human embryonic kidney 293 cells, using intracellular fluorescence measurements of BCECF, to monitor intracellular pH. CAXIV increased the rate of AE3fl-mediated HCO_3^- transport by up to 120%, which was suppressed by the CA inhibitor acetazolamide. Association of AE3 and CAXIV may represent a mechanism to enhance disposal of waste CO_2 and to balance pH in excitable tissues.

bicarbonate transport metabolon; AE3/CAXIV complex; central nervous system

MAINTENANCE OF HCO_3^- HOMEOSTASIS, extracellular pH (pH_o), and the buffer capacity of extracellular fluids are essential for cell survival. In addition, cellular processes are directly affected by modification of the intracellular pH (pH_i) (40). Brain and heart are excitable tissues that require tight control of both pH_o and pH_i. In the brain, neuronal activity has been observed upon shift of pH_o (7); neuronal activity triggers changes in pH_o and pH_i (6, 7). Given the sensitivity of many ion channels to H^+, modulation of local pH may influence neural function, particularly where pH shifts are sufficiently large and rapid (6). Na^+/H^+ exchanger (20), Na^+-driven Cl^-/HCO_3^- exchanger (33), Na^+-HCO_3^- cotransport (38), and Na^+-independent Cl^-/HCO_3^- exchanger (AE) (18) are all involved in the regulation of pH_i in brain.

The AE family comprises three genes: AE1, AE2, and AE3 (5). The AE3 gene *(SLC4A3)* encodes full-length AE3 (AE3fl) and the cardiac AE3 (AE3c) generated by alternative promoter usage (45). The AE3c polypeptide is 1030 amino acids long (~120 kDa), whereas the AE3fl variant consists of 1227 amino acids (~160 kDa). The COOH-terminal 957 amino acids of both polypeptides are identical, but AE3c contains a unique NH_2-terminal sequence of 73 amino acids in place of the first 270 amino acids of AE3fl. AE3 catalyzes electroneutral Cl^-/HCO_3^- exchange across cell membranes, regulating $[Cl^-]_i$, $[HCO_3^-]_i$, pH_i, and cell volume (5). Excitable (neuron) and support (glial) brain cells express only the ~160 kDa AE3fl isoform (15), while inner retina, which is also part of the central nervous system (CNS), expresses both AE3fl and AE3c isoforms, in neuronal and glial cells (14).

Cl^-/HCO_3^- exchange by AE3, well documented in the myocardium (8), is important for normal pH regulation (17) and is disrupted in pathological conditions (9, 31, 48). Myocardial pH_i is tightly controlled since cardiac contractility is directly affected by changes in pH_i (10). Moreover, deviations of normal pH_i have been implicated in changes of myofilament Ca^{2+} sensitivity (16, 27).

Anion exchangers associate with carbonic anhydrases (CA) to form a HCO_3^- transport metabolon, which enhances HCO_3^- flux across the plasma membrane (21). The CA family comprises 15 members, with at least 13 enzymatically active isozymes that differ in their tissue distribution and subcellular localization. The CAs have important roles in the regulation of pH, CO_2, and ion and water transport (30). CAs catalyze the reversible hydration of CO_2 to form HCO_3^- and H^+, accelerating this spontaneous reaction by up to 6,000 times. CAIV (anchored to the cell surface by a glycosylphosphatidyl inositol anchor) and CAXIV (anchored to the cell surface by a transmembrane segment) are expressed in the CNS (24, 28). These CA isoforms, with catalytic sites on the extracellular surface, are involved in regulation of brain pH_o (39). CAIV and CAXIV influence neuronal activity, reflecting the pH sensitivity of many synaptic molecules, including transporters and receptors (6). Recently, CAIX and CAXIV were found in different subcellular compartments in cardiac myocytes (37), suggesting divergent functions of the enzymes in excitation-contraction coupling.

AE3fl has a broad neuronal expression pattern and particularly strong expression in the pyramidal stratus of the hippocampus, in mouse brain (12). CAXIV is a recently identified mammalian CA isozyme, whose presence has been demon-

Address for reprint requests and other correspondence: B. V. Alvarez, Centro de Investigaciones Cardiovasculares, Facultad de Ciencias Médicas, Universidad Nacional de La Plata, 1900 La Plata, Argentina (e-mail: balvarez@med.unlp.edu.ar).

strated in different tissues, including detection in neuronal membranes and axons in both mouse and human brain by immunostaining (28). Maximum expression of CAXIV was observed in neuronal bodies and axons in pons and medulla oblongata. CAXIV is also expressed in hippocampus and other parts of mouse brain (28).

The similar tissue expression pattern and previously reported interaction of AEs and other CAs in HCO_3^- transport metabo-

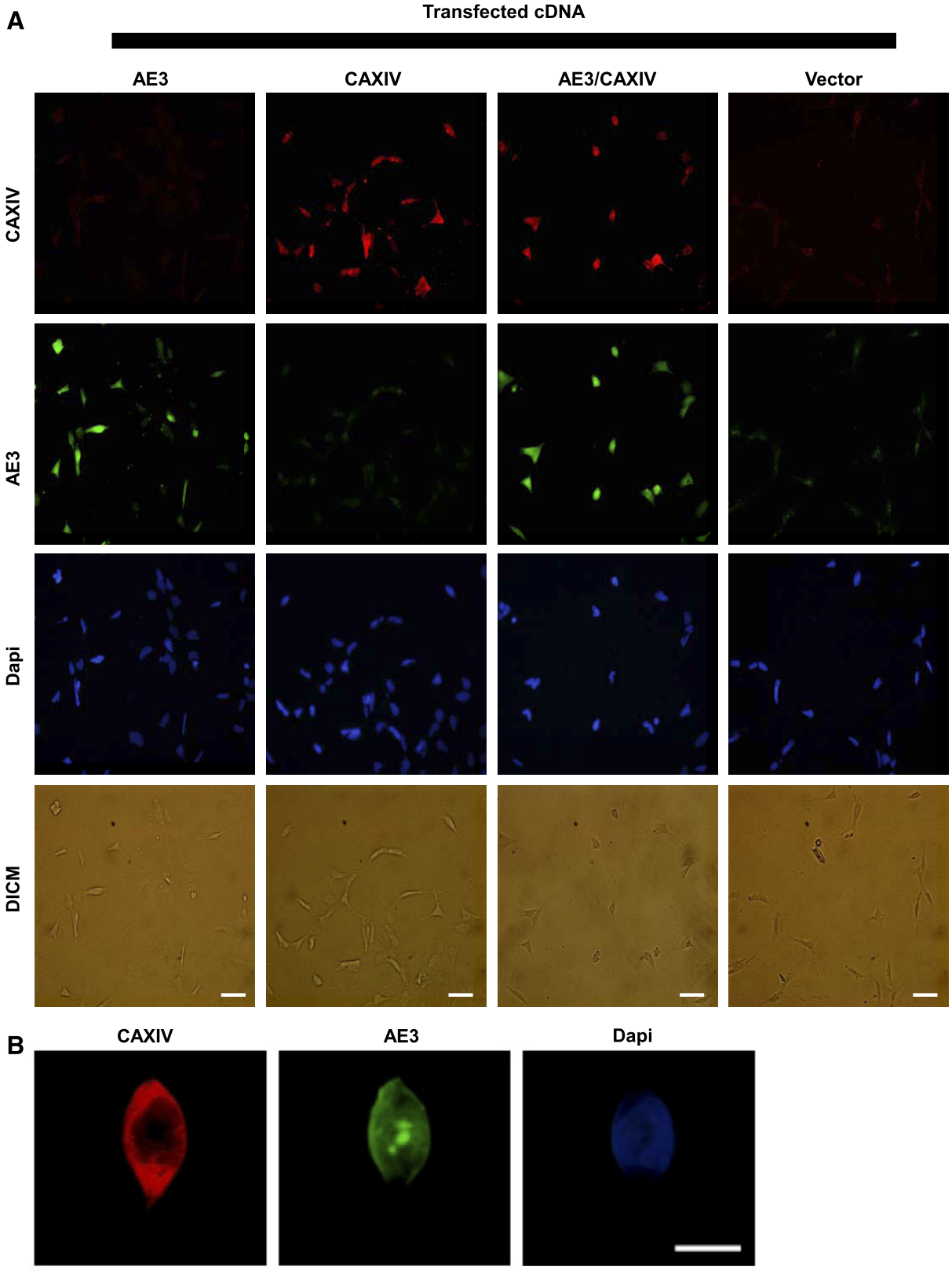

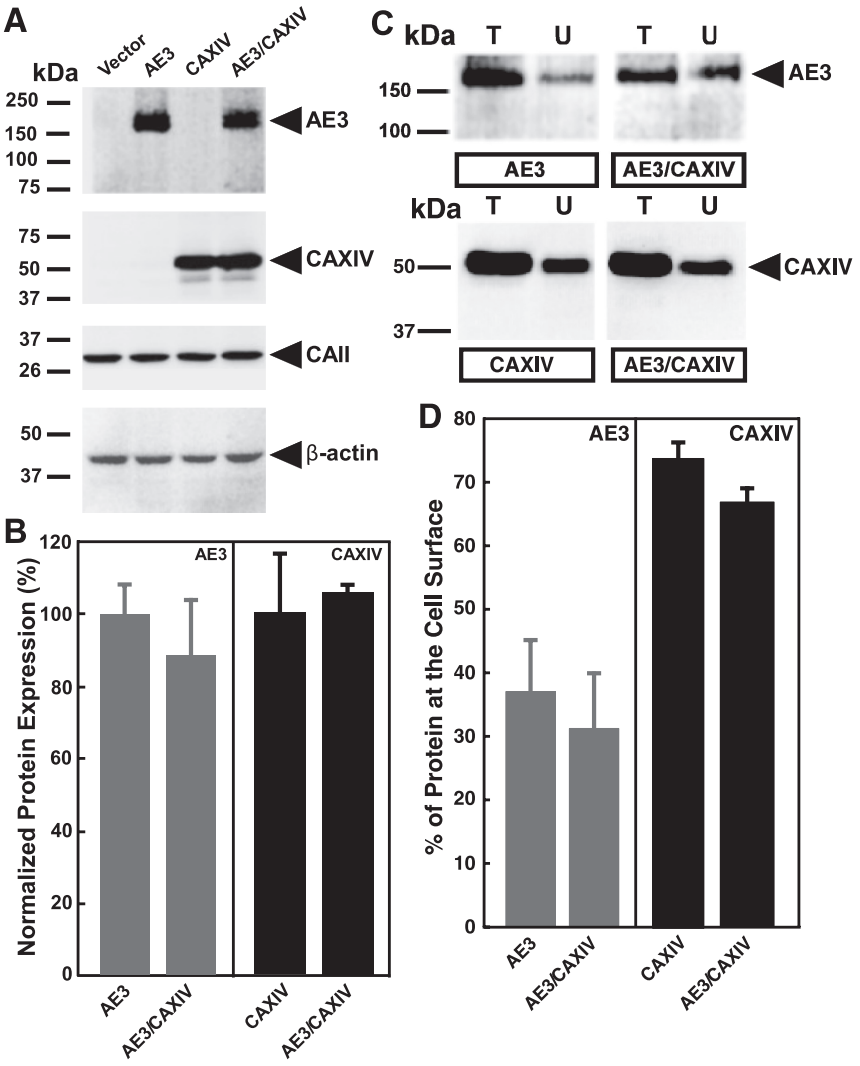

Fig. 2. Expression of AE3 and CAXIV in transiently transfected HEK293 cells and effect of CAXIV on AE3 surface targeting. *A*: HEK293 cells were either transfected with AE3, or CAXIV, cDNA, or cotransfected with AE3 and CAXIV, cDNAs. Samples were analyzed by 7.5% SDS-PAGE (*top*) or 10% SDS-PAGE (*middle* and *bottom*), transferred to polyvinylidene difluoride (PVDF) membranes, and probed with indicated antibodies directed against AE3, CAXIV, CAII, or β-actin. *B*: expression of AE3 (light-shaded bars) and CAXIV (dark-shaded bars) were quantified by densitometry and normalized to the amount of β-actin in the sample. *C*: transfected or cotransfected HEK293 cells (expressing the proteins indicated in the boxes) were incubated with membrane-impermeant Sulpho-NHS-SS-biotin. Cell lysates were prepared from the cells. Half of the cell lysate was incubated with streptavidin-Sepharose resin, which bound biotinylated proteins, representing proteins labeled at the cell surface. Material remaining in the lysate (unbound, U) represented protein that did not incorporate a biotin tag and which therefore had an intracellular localization. The remaining cell lysate (total fraction, T) was not treated with streptavidin-Sepharose and thus represented the total amount of protein in the sample. Samples of the T and U fractions were subjected to SDS-PAGE and probed on immunoblots for the presence of AE3 or CAXIV. Representative immunoblots of total and unbound fractions probed for AE3 (*top*) or CAXIV (*bottom*) are shown. *D*: summary of cell surface targeting of AE3, CAXIV, or AE3 in the presence of CAXIV. The amount of AE3 (light-shaded bars) and CAXIV (dark-shaded bars), or AE3 in the presence of CAXIV on immunoblots was quantified by densitometry. Percentage of protein at the cell surface = (T − U)/T × 100%; $n = 4$.

lons (21, 44, 46) suggested that AE3 might associate with CAXIV. AE3/CAXIV interaction could contribute to the disposition of the enormous CO_2 load generated from neuronal metabolism. Indeed, a functional coupling between CAIV and CAXIV and the AE3 Cl^-/HCO_3^- exchanger was recently demonstrated in hippocampal neurons (46).

To examine whether AE3 and CAXIV physically associate in the CNS, coimmunoprecipitation experiments were performed using lysates of mouse brain and retina. We found that CAXIV coimmunoprecipitated with anti-AE3 antibody and that AE3 could be coimmunoprecipitated using anti-CAXIV antibody. These results suggest that CAXIV and AE3 interact in the CNS. CAXIV increased the rate of AE3fl-mediated HCO_3^- transport in functional assays, indicating a functional link between CAXIV enzyme and AE3 Cl^-/HCO_3^- exchanger. The results presented in this work indicate that the AE3/CAXIV metabolon constitutes a system to dispose of high CO_2 and H^+ production and to regulate pH in brain and retina.

MATERIALS AND METHODS

Animals. Knockout mice used for this study were produced through targeted mutagenesis of caXIV (39), and ae3 (1), as previously described. Animal protocols were approved by the University of Alberta Animal Policy and Welfare Committee and were performed in accordance with Canadian Council on Animal Care guidelines.

Preparation of mouse retinal and brain lysates and human embryonic kidney 293 cell lysates. Mice were euthanized by an overdose of Euthanyl (pentobarbital sodium) administered intraperitoneally. One brain was rapidly explanted out and placed in 4 ml ice-cold IPB buffer (1% Igepal, 5 mM EDTA, 0.15 M NaCl, 0.5% deoxycholate, 10 mM Tris·HCl, pH 7.5), containing 2 mg/ml BSA and protease inhibitors (PI, MiniComplete Tablet, Roche). Tissue was disrupted in a Polytron

Fig. 1. Immunocytochemical analysis of human embryonic kidney (HEK)293 cells expressing full-length anion exchanger 3 (AE3fl) and carbonic anhydrase (CA) XIV proteins. *A*: HEK293 cells plated on glass coverslips were transfected with AE3fl, CAXIV, AE3fl and CAXIV cDNAs or empty vector cDNAs *(top)*. Cells were stained as indicated on the *left* side, with rabbit anti-AE3 antibody, followed by Alexa Fluor 488-conjugated chicken anti-rabbit IgG secondary antibody (AE3, green) or with goat anti-CAXIV antibody, followed by Alexa Fluor 594-conjugated chicken anti-goat IgG (CAXIV, red). Nuclei were stained with DAPI. Images were collected with an Olympus Bx51 microscope and captured with an Olympus DP70 cooled digital color camera. Scale bar = 40 μm. DICM, differential interference contrast microscopy. *B*: double images of higher magnifications of CAXIV (red) and AE3 (green) in HEK293 cells transfected with constructs encoding CAXIV and AE3. Nuclei were stained with DAPI (blue). Scale bar = 10 μm.

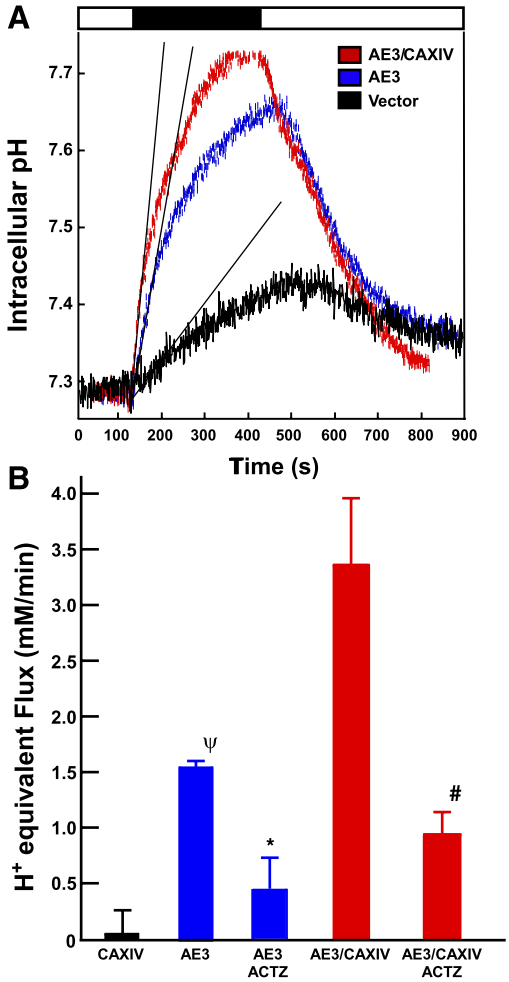

Fig. 3. Effect of CAXIV on AE3 transport activity. HEK293 cells transiently transfected with pRBG4 (vector), AE3, or CAXIV cDNA, or cotransfected with AE3 and CAXIV, cDNAs, were loaded with BCECF-AM and placed into a fluorimeter to monitor intracellular pH (pH_i). *A*: cells were perfused alternately with Cl^--containing (open bar) and Cl^--free (black bar) Ringer buffer. Initial rates of change of pH_i during the first minute were estimated from the slope of the line fitted by least squares method (straight black lines). *B*: summary of transport activity for HEK293 cells expressing CAXIV and AEs, as indicated. Transport activity was calculated after subtraction of proton flux corresponding to cells transfected with empty vector. Transport activity of cells expressing AE3, or AE3 and CAXIV was normalized to the amount of AE3 protein expressed at the cell surface. Some rates represent data collected in the presence of 150 μM acetazolamide (ACTZ), as indicated. *Statistical significance ($P < 0.05$) compared with AE3. #,ψStatistical significance ($P < 0.05$) compared with AE3/CAXIV; $n = 4$ for all data.

(Kinematica) and kept on ice for 10 min. Freshly isolated mouse retinas were homogenized by 12 strokes of a Dounce homogenizer in 0.5 ml/retina of ice-cold IPB buffer containing PI (500 μg of total protein), or cells grown on 60-mm Petri dish were disrupted with a cell scraper in 250 μl of IPB buffer, containing PI (250 μg total protein). Disrupted retinal tissue and human embryonic kidney (HEK)293 cells were incubated on ice for 10 min.

Protein expression. Expression constructs for human CAII (44), human CAIV (54), human CAIX (29), human CAXII (47), mouse CAXIV (28), rat AE3 full-length (AE3fl) (43), and enhanced green fluorescent protein (eGFP) (53), have been described previously. HEK293 cells were individually transfected with empty vector (pRBG4 or pCDNA3, as indicated), CAII, CAIV, CAIX, CAXII, CAXIV, or AE3fl, or individually cotransfected with CAXIV and AE3fl, cDNAs, using the calcium phosphate method (34). Cells were grown at 37°C in an air-CO_2 (19:1) environment in DMEM medium, supplemented with 5% (vol/vol) fetal bovine serum and 5% (vol/vol) calf serum.

Immunodetection. Two days posttransfection, cells were washed in PBS buffer (140 mM NaCl, 3 mM KCl, 6.5 mM Na_2HPO_4, and 1.5 mM KH_2PO_4, pH 7.5) and cell lysates were prepared by addition of 150 μl SDS-PAGE sample buffer to 60-mm Petri dish. Samples (50 μg protein) were resolved by SDS-PAGE on 7.5–10% acrylamide gels, as indicated. Proteins were transferred to polyvinylidene difluoride membranes and then incubated with rabbit anti-AE3 (55) (SA8, 1:2,000 dilution), goat anti-CAXIV (N-19, 1:500; Santa Cruz), goat anti-CAII (C-14, 1:500; Santa Cruz), goat anti-CAIV (N-16, 1:500; Santa Cruz), mouse anti-CAIX (22), or mouse anti-HA hemagglutinin tag antibody (1:1,000 dilution, Covance). Immunoblots were then incubated with 1:1,000 dilution of donkey anti-rabbit IgG (Santa Cruz), or mouse anti-goat IgG (Santa Cruz), or sheep anti-mouse IgG (NA931V, Amersham Biosciences), conjugated to horseradish peroxidase. Blots were visualized and quantified using enhanced chemiluminescence reagent and a Kodak Image Station.

Coimmunoprecipitation. Homogenates of brain, or retinas, or HEK293 cell lysates, were centrifuged at 1,440 *g* for 5 min in a Beckman G5–6K centrifuge. Supernatants (3.5 ml corresponding to a total of ~1.7 mg of protein of brain lysate) were removed and applied to 50 μl protein G-Sepharose (50% slurry) for 3 h at 4°C. After centrifugation (5 min, 8,000 *g*), lysates were incubated overnight with goat polyclonal anti-CAXIV antibody (6 μl, 1.2 μg IgG), or nonimmune goat serum (6 μl), or rabbit polyclonal anti-AE3 antibody (43) (AP3, 5 μl, 1.5 μg IgG), or mouse monoclonal anti-HA hemagglutinin tag antibody (2 μl, 2.0 μg IgG), and 100 μl protein G-Sepharose (at 4°C, overnight). Resin was washed consecutively with *wash 1* (0.1% Igepal, 1 mM EDTA, 0.15 M NaCl, and 10 mM Tri·HCl, pH 7.5), *wash 2* (2 mM EDTA, 0.05% SDS, and 10 mM Tri·HCl, pH 7.5), and *wash 3* (2 mM EDTA and 10 mM Tri·HCl, pH 7.5). After centrifugation (2,000 *g*), resin was resuspended in an equal volume of 2× SDS-PAGE sample buffer. Samples were electrophoresed on 7.5% or 10% acrylamide gels, as indicated. Immunoblots were probed with anti-AE3 antibody (SA8, 1:2,000 dilutions) or anti CAXIV antibody (1:500 dilutions).

Immunostaining of mouse retinas. For immunofluorescence experiments, mice were euthanized with high-dose Euthanyl and their eyes removed and immediately frozen at −80°C in Shandon Cryomatrix (Thermo Electron). Cryostat sections (20 μm thick) of retinas were then cut onto glass slides. Following washing (2 × 5 min with PBS), and blocking (10% chicken serum in PBS, 30 min), retina sections were incubated with primary antibodies in PBS buffer containing 0.5% (vol/vol) Triton X-100 (overnight, in a humidified chamber, 25°C), washed (3 × 5 min in PBS), and incubated with secondary antibody as above (1 h, in a humidified chamber, 25°C). Primary rabbit polyclonal anti-AE3 (AP3) (43) antibody, rabbit anti-AE3c (43), goat anti-vimentin (C-20, Santa Cruz), goat anti-glial fibrillary

Table 1. *Cl^-/HCO_3^- exchange activity*

Cell Transfection/ACTZ Added	Bicarbonate Influx, mM/min	Bicarbonate Efflux, mM/min
AE3	1.5±0.1†	1.5±0.3†
AE3 + 150 μM ACTZ	0.4±0.3*	0.5±0.3*
AE3/CAXIV	3.4±0.6	3.4±0.5
AE3/CAXIV + 150 μM ACTZ	0.9±0.2†	1.4±0.4†

Anion exchange rates measured during Cl^- removal (bicarbonate influx) and Cl^- addition (bicarbonate influx) are shown as means ± SE for $n = 4$ experiments. All rates are corrected for background rates of cells transfected with empty vector and were normalized for the amount of AE3 protein expressed at the cell surface. ACTZ, acetazolamide; CA, carbonic anhydrase. *Statistical significance ($P < 0.05$) compared with AE3. †Statistical significance ($P < 0.05$) compared with AE3/CAXIV.

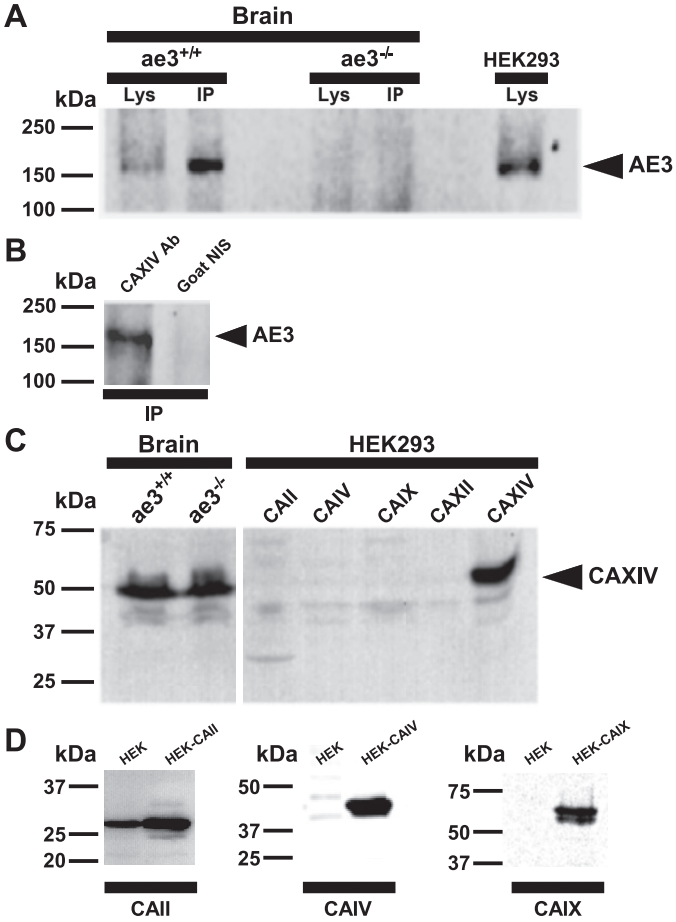

Fig. 4. Coimmunoprecipitation of AE3/CAXIV complex from mouse brain. *A*: a total of 1,700 μg protein of mouse brain lysates from ae3$^{+/+}$ or ae3$^{-/-}$ mutant mice were immunoprecipitated (IP) with goat polyclonal antibody directed against CAXIV and resuspended in a final volume of 100 μl. The gels were loaded with lysates, corresponding to 25 μg of protein and 100 μg of immunoprecipitated protein (50 μl). Brain lysate (Lys and IP) and lysate from AE3-transfected HEK293 cell lysates were electrophoresed on 7.5% acrylamide gels, transferred to a PVDF membrane, and probed on with anti-AE3 rabbit polyclonal antibody (SA8). *B*: brain lysates of ae3$^{+/+}$ mice were immunoprecipitated with goat polyclonal CAXIV antibody or immunoprecipitated with irrelevant goat nonimmune serum (NIS). Electrophoresed and transferred samples were probed on with anti-AE3 antibody. *C*: brain lysates, or HEK293 cells transfected with CAII, CAIV, CAIX, CAXII, or CAXIV, cDNAs, were analyzed on 10% acrylamide gels, transferred to PVDF membranes, and probed with anti-CAXIV antibody. Position of AE3 and CAXIV is shown (filled arrow). Samples were all analyzed on the same gel. *D*: lysates of untransfected HEK293 cells or HEK293 cells transfected with CAII, CAIV, or CAIX, cDNAs, were analyzed on 10% acrylamide gels, transferred to PVDF membranes, and probed with the antibodies indicated across the *bottom*.

acidic protein (GFAP; C-19, Santa Cruz), goat anti-CAXIV (N-19, Santa Cruz), and goat anti-calbindin (C-20, Santa Cruz) were used at 1:100 dilution. Secondary chicken anti-rabbit conjugated to Alexa Fluor 488 (green), or secondary goat anti-rabbit conjugated to Alexa Fluor 488 (green), or secondary goat anti-mouse conjugated to Alexa Fluor 594 (red) were used at 1:200 dilutions. Slides were washed three times in PBS and mounted and viewed using confocal microscopy.

Imaging and analysis by confocal microscopy. Immunostained retinas on slides were mounted in Prolong Anti-fade solution containing DAPI for nuclei staining (Molecular Probes, Eugene, OR). Retinal sections on slides were imaged with a Zeiss LSM 510 laser-scanning confocal microscope imaging system mounted on an Axiovert 100M controller. Images were collected using an oil immersion ×43 objective (retinas), or collected with an oil immersion ×63 objective (numerical aperture 1.4, plan Apochromat) at a resolution of 0.5- to 0.7-μm field depth. Filtering was used to integrate the signal collected over 4–8 frames to decrease noise (scan time = 7 s/frame). Multiple retinal sections from different mice were studied.

Cl^-/HCO_3^- exchange assays. HEK293 cells, grown on 6 × 11 mm glass, were transfected with cDNAs. Two days posttransfection, coverslips were incubated in serum-free DMEM containing 2 μM BCECF-AM (Molecular Probes) at 37°C for 20 min. Coverslips in a fluorescence cuvette were perfused at 3.5 ml/min alternately with Ringer buffer (5 mM glucose, 5 mM potassium gluconate, 1 mM calcium gluconate, 1 mM $MgSO_4$, 2.5 mM, NaH_2PO_4, 25 mM $NaHCO_3$, and 10 mM HEPES, pH 7.40), containing either 140 mM NaCl (Cl^--containing) or 140 mM sodium gluconate (Cl^--free). Both buffers were continuously bubbled with air-5% CO_2. Fluorescence changes were monitored in a Photon Technologies International RCR fluorimeter at excitation wavelengths of 440 and 502 nm and emission wavelength of 528 nm. All transport data were corrected for background activity of HEK293 cells transfected with vector alone. Intrinsic buffer capacity (β_i) was negligible at pH_i values above 7.10 (43), so that $\beta_{total} = \beta_{CO2}$, where $\beta_{CO2} = 2.3 \times [HCO_3^-]$. Total flux of proton equivalents was calculated as $J_{H+} = \beta_{total} \times \Delta pH_i$ (33), where pH_i was determined by linear regression of the first minute of alkalinization, using Kaleidagraph software, and fluxes are expressed as mM H^+/min.

Cell surface targeting assays. AE3 and CAXIV proteins were individually expressed or coexpressed by transient transfection of HEK293 cells, with cDNAs, using the calcium phosphate method (34). Cells were grown at 37°C in an air-CO_2 (19:1) environment in DMEM medium, supplemented with 5% (vol/vol) fetal bovine serum and 5% (vol/vol) calf serum. Assays to assess the degree of cell surface targeting and biotinylation of AE3 and CAXIV proteins were performed as follows. Briefly, cells were labeled with membrane-impermeant Sulpho-NHS-SS-biotin and then solubilized in lysis buffer. Half of the cell lysate was incubated with streptavidin-Sepharose resin, which bound biotinylated proteins. Unbound protein fraction did not incorporate a biotin tag and therefore had an intracellular localization. Cell lysate total fraction was not treated with streptavidin-Sepharose, therefore representing the total amount of protein in the sample. Samples of the total and unbound fractions were subjected to SDS-PAGE and probed on immunoblots for the presence of AE3, or CAXIV, and the amount of AE3 and CAXIV on blots was quantified by densitometry, using a Kodak Image Station.

Immunostaining of HEK293 cells. Cells grown on 22 × 22 mm laminin (30 μg/ml)-coated coverslips were transiently transfected as described above. Cells were washed in PBS and fixed for 20 min in 4% (wt/vol) paraformaldehyde in PBS. After three washes with PBS, the cells were incubated for 2 min in PBS, containing 0.1% (vol/vol) Triton X-100. Slides were blocked for 25 min with PBSG [0.2% (wt/vol) gelatin in PBS] and incubated with a 1:500 dilution of goat anti-CAXIV antibody (Santa Cruz), and rabbit polyclonal anti-AE3 antibody (AP3, 1:500 dilution) for 1 h in a humidified chamber at room temperature. After three washes with PBSG, coverslips were incubated for 1 h in a dark humidified chamber with a 1:250 dilution of Alexa Fluor 594-conjugated chicken anti-goat IgG, and with Alexa Fluor 488-conjugated chicken anti-rabbit IgG. Coverslips were mounted in Prolong Gold Antifade Solution containing DAPI (Molecular Probes) and fluorescent images were obtained with an Olympus Bx51 microscope. Images were captured with an Olympus DP70 cooled digital color camera and collected with an Uplan FLN ×40 objective. Higher-magnification images were collected with an Uplan Apo ×100/1.35 objective.

Statistical analysis. Statistical significance was evaluated using unpaired or paired *t*-test and one-way ANOVA. $P < 0.05$ was considered significant. Error bars show standard error of the mean.

RESULTS

Expression of AE3fl and CAXIV in HEK293 cells. HEK293 cells were individually transiently transfected with empty vector cDNA, AE3fl cDNA, or CAXIV cDNA, or were cotransfected with AE3fl and CAXIV, cDNAs. To determine transfection efficiency, we performed immunocytochemical analysis of transfected HEK293 cells.. Transfection efficiency was estimated as the number of fluorescent cells (red or green) relative to the number of total cells (DAPI) taken in three separate fields and expressed as a percentage. Transfection efficiency for AE3fl and CAXIV was similar, whether expressed alone (50 ± 3% and 49 ± 2%, respectively) or together (48 ± 3%), as visualized by fluorescence of transfected cells. Cells transfected with empty vector had only low levels of background fluorescence (Fig. 1*A*). CAXIV protein localizes predominantly at the border of the cell, as expected for a membrane-bound protein, whereas AE3 protein localizes at the cell border and in cytoplasmic locations to some extent, presumably as a consequence of retention in the endoplasmic reticulum (Fig. 1*B*).

The expression of AE3fl and CAXIV was further explored on immunoblots. Transfected HEK293 cells were solubilized, and samples were analyzed by SDS-PAGE, blotted, and probed for the level of AE3fl and CAXIV expression (Fig. 2, *A* and *B*). Expression of AE3fl and AE3fl/CAXIV was normalized to the amount of β-actin. CAII, which is endogenously expressed in HEK293 cells, did not change expression among the different samples, when normalized to β-actin (not shown). Expression of CAXIV, normalized to β-actin, was similar in cells expressing CAXIV alone, or coexpressing CAXIV and AE3fl (Fig. 2*B*), but expression of AE3fl in cells cotransfected with AE3fl and CAXIV cDNA was slightly reduced (12%) compared with those expressing AE3fl alone (Fig. 2*B*).

To investigate the effects of CAXIV on AE3 cell surface targeting, we expressed AE3fl either alone or with CAXIV in HEK293, and we determined the degree to which CAXIV could be labeled with membrane-impermeant Sulpho-NHS-SS-biotin. Cells were labeled with Sulpho-NHS-SS-biotin and then solubilized in lysis buffer. Samples were incubated with streptavidin resin to remove biotinylated proteins, leaving the unbound fraction. Samples of total (T) and unbound (U) fractions were subjected to SDS-PAGE and probed on immunoblots for the presence of AE3fl or CAXIV. The amount of AE3fl and CAXIV on the blots was quantified by densitometry (Fig. 2, *B* and *D*, $n = 4$). The fraction of protein that was biotinylated is interpreted as localized to the cell surface, because it is accessible to labeling by the membrane-impermeant biotinylation reagent. We estimated the fraction of biotinylated protein as: $(T - U)/T$.

The fraction of AE3fl at the cell surface was 37 ± 9% for AE3 alone, which was statistically indistinguishable from

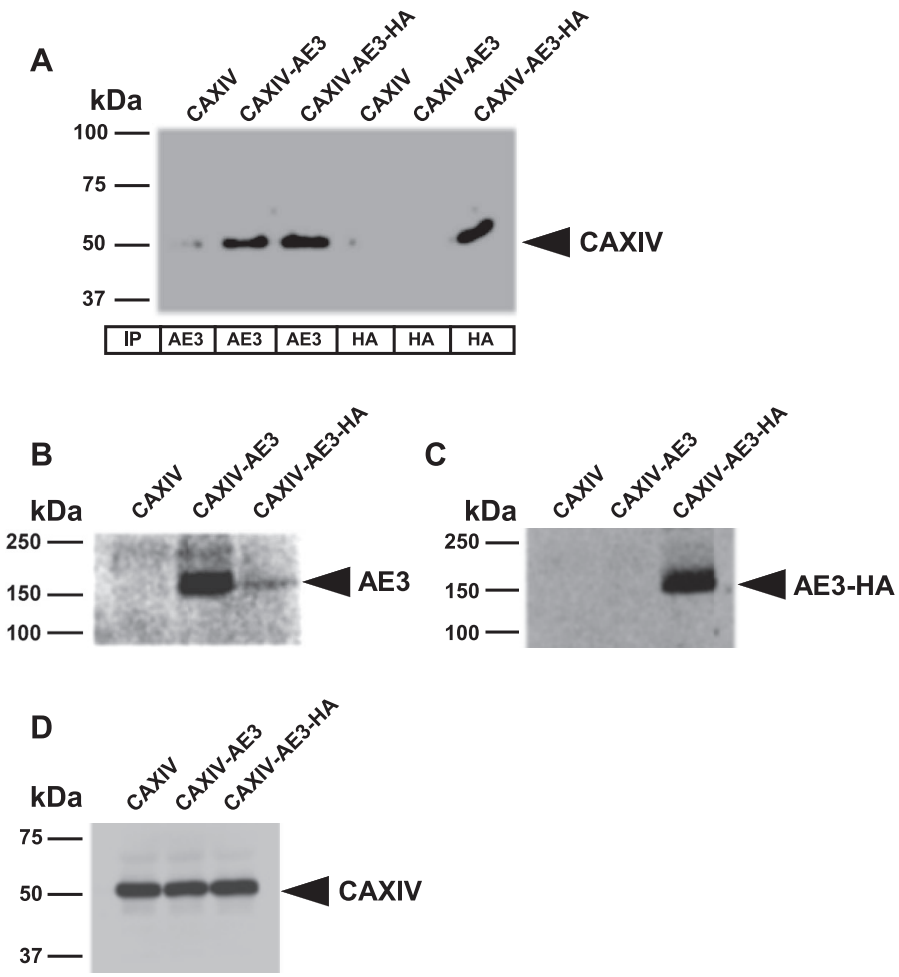

Fig. 5. Coimmunoprecipitation of AE3 and CAXIV coexpressed in HEK293 cells. HEK293 cells were transiently transfected with CAXIV cDNA or cotransfected with CAXIV and AE3 cDNAs, or CAXIV and AE3 tagged with a hemagglutinin (HA) epitope tag (AE3-HA), cDNAs. *A*: cell lysates were prepared from cells transfected with the cDNAs labeled across the *top*. Lysates were immunoprecipitated with anti-AE3 antibody or anti-HA antibody (indicated across the *bottom*), resolved by SDS-PAGE, blotted, and probed with an anti-CAXIV antibody. *B–D*: lysates, resolved by SDS-PAGE and blotted to PVDF membrane, were probed on immunoblots with anti-AE3 (*B*), AE3-HA (*C*), or anti-CAXIV antibody (*D*).

AE3fl in AE3fl/CAXIV-cotransfected cells (32 ± 9%). In parallel experiments we found that the cell surface fraction of CAXIV was 74 ± 2% for CAXIV alone and 67 ± 2% for AE3fl/CAXIV. To assess the validity of this approach, in a separate experiment (not shown), we determined whether a cytosolic marker protein, eGFP, could be labeled by Sulpho-NHS-SS-biotin. In two separate determinations, only ~4% of eGFP was labeled with biotin, indicating that the biotinylation protocol is reliable in labeling little cytosolic protein.

Functional complex of AE3 Cl^-/HCO_3^- exchanger and carbonic anhydrase XIV. To explore the effect of CAXIV on AE3-mediated Cl^-/HCO_3^- exchange activity, HEK293 cells were transiently transfected with cDNAs encoding AE3fl, CAXIV, and pRBG4 (empty vector), or cotransfected with both CAXIV and AE3fl, cDNAs. HEK293 cells express low endogenous Cl^-/HCO_3^- exchange activity (41). Cells were loaded with the pH-sensitive dye BCECF-AM and were perfused alternately with Ringer buffer containing 140 mM NaCl and Ringer buffer lacking Cl^-. Bicarbonate transport was monitored by measurements of pH_i upon changes on transmembrane [Cl^-] gradient. Transport rates were determined by initial rate of change of pH_i following changes of perfusion buffer. Background activity was examined in HEK293 cells transfected with empty vector, and the transport activity calculated for CAXIV, AE3, and AE3-CAXIV was corrected for vector alone (Fig. 3*A*). Cells transfected with vector cDNA displayed 35% of Cl^-/HCO_3^- exchange activity, compared with cells transfected with AE3fl (0.9 ± 0.2 mM H^+/min vs. 2.3 ± 0.1 mM H^+/min, respectively, $n = 4$) (Table 1). Coexpression of AE3 with CAXIV significantly increased AE3-mediated HCO_3^- transport activity by ~65% (Fig. 3*B*). Interestingly, expression of CAXIV alone did not affect the background transport rate (0.8 ± 0.5 mM H^+/min, $n = 4$), thus indicating that the CAXIV effects were dependent on the presence of AE3 (Fig. 3*B*).

The role of CAXIV in determining the rate of Cl^-/HCO_3^- exchange activity by AE3 was studied in the absence and presence of 150 μM acetazolamide (ACTZ). ACTZ is a membrane-permeant carbonic anhydrase inhibitor, which does not act directly on AE1, rather mediating its effects on carbonic anhydrase (23).

Cl^-/HCO_3^- exchange activity in AE3fl-transfected HEK293 cells was reduced by 70% by ACTZ (0.4 ± 0.3 mM H^+/min, $n = 4$). The inhibition of Cl^-/HCO_3^- exchange activity in AE3fl-alone-transfected cells (Fig. 3*B*) suggests that AE3 transport activity is accelerated by the presence of endogenous CAII. In cells expressing both AE3fl and CAXIV, ACTZ inhibited Cl^-/HCO_3^- exchange activity by 80%, demonstrating a functional coupling between AE3 and CAXIV.

CAXIV expression could affect AE3 transport rate by altering the efficiency of AE3 targeting to the plasma membrane. Therefore, transport rates were corrected for the abundance of AE3 at the plasma membrane. Transport activity of HEK293 cells expressing AE3 and CAXIV, corrected to AE3 expressed at the cell surface, increased by 120% compared with AE3 alone (3.4 ± 0.6 mM H^+/min, $n = 4$, Fig. 3*B*). Cl^-/HCO_3^- exchange activity in HEK293 cells cotransfected with AE3fl and CAXIV, cDNAs, was inhibited with the potent CA inhibitor ACTZ, by 70% (0.9 ± 0.2 mM H^+/min, $n = 4$, Fig. 3*B*), when corrected to protein present at the cell surface.

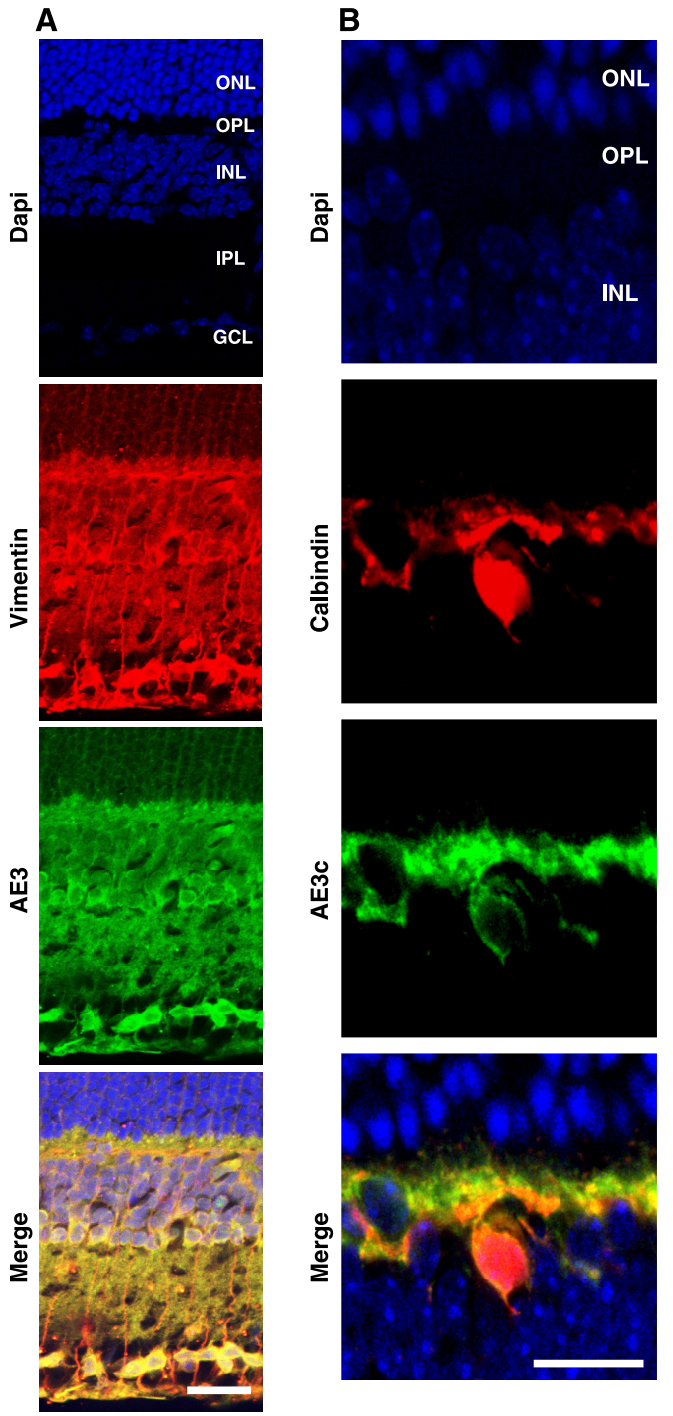

Fig. 6. Localization of AE3 in adult mouse retina. Frozen vertical sections of mouse retina were labeled with anti-AE3 (AP3) or anti AE3c antibodies. *A* and *B*: colocalization of AE3 immunofluorescence with intermediate filaments in inner retina was visualized by double-labeling of AE3 antibodies and specific markers of retinal Müller cells (vimentin), and retinal horizontal cells (calbindin). Immunofluorescence signals were visualized by Alexa Fluor 488-conjugated anti-rabbit IgG antibody (green, 1:100 dilution) and Alexa Fluor 594-conjugated anti-goat IgG antibody (red, 1:100 dilution). Sections were also stained with DAPI to identify nuclei. Images were collected with a Zeiss LSM 510 laser-scanning confocal microscope with ×40/1.3 oil immersion objective (Neofluar oil differential interference contrast). Colocalization of AE3 and vimentin, and AE3c and calbindin, with yellow staining in merge panel. Scale bar = 25 μm. ONL, outer nuclear layer; OPL, outer plexiform layer; INL, inner nuclear layer; IPL, inner plexiform layer; GCL, ganglion cell layer.

Cl^-/HCO_3^- exchange activity by AE3 was also estimated after reintroduction of extracellular chloride, when AE3 mediates HCO_3^- efflux (Table 1). The rates were very similar to those obtained after chloride removal. Coexpression of CAXIV and AE3 increased the AE3-mediated HCO_3^- transport when chloride was reintroduced to the media. Therefore, the stimulatory effect that CAXIV conferred on AE3 by CAXIV did not differ depending on ion transport direction.

AE3 Cl^-/HCO_3^- exchanger and CAXIV physical association. Physical interactions between AE3 Cl^-/HCO_3^- exchangers and CAXIV were next explored in mouse tissues. We first studied physical interactions between AE3 and CAXIV in mouse brain by coimmunoprecipitation.

CAXIV from whole mouse brain lysates was immunoprecipitated using anti-CAXIV antibody, and corresponding immunoblots were probed with a rabbit anti-AE3 COOH-terminal antibody. The anti-AE3 antibody recognized a ~160 kDa band in wild-type $ae3^{+/+}$ mouse brain lysates and HEK293 cell lysates expressing AE3 (Fig. 4*A*). Importantly, immunoreactive material at 160 kDa was not seen in lysates from $ae3^{-/-}$ (mouse with a targeted disruption of the ae3 gene) brain lysates. Anti-CAXIV antibody was able to coimmunoprecipitate the AE3fl isoform from $ae3^{+/+}$ mouse (Fig. 4, *A* and *B*). Coimmunoprecipitation experiments performed on brain lysates obtained from $ae3^{-/-}$, which does not express AE3 protein, failed to pull down AE3 with the CAXIV antibody (Fig. 4*A*), indicating specificity of the immunoprecipitation. Similarly, nonimmune goat serum failed to coimmunoprecipitate AE3 and CAXIV (Fig. 4*B*).

Expression of CAXIV was detected in whole brain lysate from both $ae3^{+/+}$ and $ae3^{-/-}$ mice on immunoblots probed with the same antibody used for coimmunoprecipitation studies (Fig. 4*C*). The amino acid sequence identity of human CAXIV relative to the other membrane-associated isozymes (CAIV, CAIX, and CAXII) is 34–46%. Conversely, amino acid identity of human CAXIV and CAII is only 27%. CAXIV antibody used for immunoprecipitation showed minimal to no cross-reaction with CAII, CAIV, CAIX, or CAXII transiently expressed in HEK293 cells (Fig. 4*C*). Immunoblots of HEK293 cell lysates prepared from cell transfected with CAII cDNA, or transfected with CAIV cDNA, or CAIX cDNA, and detected with specific antibodies to each CA isoforms, is shown in Fig. 4*D*, confirming that these CA isoforms were expressed upon transfection. Untransfected HEK293 cells display undetectable labels of CAIV and CAIX. Expression of CAXII could not be assessed because of difficulties with the anti-CAXII antibody (not shown).

Reciprocal AE3/CAXIV coimmunoprecipitation experiments were conducted in transfected HEK293 (Fig. 5). Anti-AE3 and anti-HA antibodies were able to precipitate CAXIV, and this was fully dependent on AE3fl and AE3-HA expression, respectively (Fig. 5, *A–C*). CAXIV was equally expressed in cells cotransfected with AE3fl and CAXIV, or cells cotransfected with AE3-HA and CAXIV, cDNAs (Fig. 5*B*). Rabbit anti-AE3 antibody, which recognized both AE3 and AE3-HA proteins, showed a more intense band for AE3 than AE3-HA on immunoblots, suggesting an interference of the COOH-terminal HA tag and the COOH-terminal epitope (Fig. 5*D*). These experiments revealed that CAXIV forms a complex with AE3 in cotransfected HEK293 cells.

Retinal AE3/CAXIV complex. The mammalian inner retina expresses AE3fl in Müller cells and AE3c horizontal neurons (14). Double-labeling immunostaining of frozen vertical retina sections from adult mice, combined with confocal immunofluorescence microscopy, was used to reexamine the expression of the two alternate AE3 proteins. Vimentin, an intermediate filament protein present in rodent retinal Müller and horizontal cells; GFAP (not shown), which labels the two major classes of retinal microglia, astrocytes and Müller cells; and calbindin, a Ca^{2+}-binding protein that labels the processes and the soma of horizontal cells in the outer plexiform layer (OPL), were used as markers to define the localization of AE3fl and AE3c (Fig. 6, *A* and *B*). Confocal images confirmed expression of the two AE3 proteins in different cell subtype populations of the inner retina. AE3c colocalized with calbindin in horizontal cells [somas in inner nuclear layer (INL) and processes in OPL], whereas both AE3c and AE3fl colocalized with vimentin and GFAP (not shown) in horizontal cells (somas in INL and processes in OPL), and Müller cells (somas and processes in the INL, and processes in the inner plexiform layer). Interestingly, AE3 also showed extensive labeling and colocalization with vimentin and GFAP (not shown) of somas present in the ganglion cell layer of mouse retinas (Fig. 6*A*).

Specificity of the AE3, calbindin, vimentin, and GFAP signals in retina sections was shown by the absence of labeling in samples treated only with secondary antibody (not shown).

CAXIV has been detected only in glial cells but not in neurons, in the mouse retina (24). In addition, CAXIV is strongly expressed on retinal pigment epithelium (RPE). The specific membrane domains that express CAXIV were end-foot and non-end-foot membranes on Müller cells, astrocytes, and apical and basolateral membranes of RPE (24). The limited location of CAXIV suggests a specialized role in buffering pH and volume in retinal neurons and their surrounding extracellular spaces.

Colocalization of AE3 and CAXIV in structures of the inner retina suggested that the AE3 Cl^-/HCO_3^- exchanger and the CAXIV enzyme might form a physical complex to maximize HCO_3^- fluxes and regulate intracellular and extracellular pH in the highly metabolic retinal tissue. Coimmunoprecipitation experiments were conducted on lysates of mouse retinas, using anti-CAXIV and AE3 antibodies (Fig. 7). AE3 antibody detected both AE3fl and AE3c isoforms in wild-type tissue. Expression of AE3 proteins was not detected in $ae3^{-/-}$ mouse retinal lysates. Wild-

Fig. 7. Analysis of AE3 and CAXIV physical complex in mouse retina. *A*: retinal lysates from $ae3^{+/+}$ or $ae3^{-/-}$ mice were electrophoresed on 7.5% (*left*) or 10% (*right*) acrylamide gels, and corresponding immunoblots were probed with anti-AE3 or anti-CAXIV antibodies, respectively. Data are representative of experiments repeated three times. Position of AE3fl (gray arrow), AE3c (white arrow), and CAXIV (black arrow) is shown. *B*: retinas of wild-type mice (*top*), or $ae3^{-/-}$-null mice (*middle*), or $caXIV^{-/-}$-null mice (*bottom*) were labeled with rabbit polyclonal anti-AE3 antibody and goat polyclonal anti-CAXIV antibody, as indicated at the *top*. Immunofluorescence signals were visualized by Alexa Fluor 488-conjugated anti-rabbit IgG antibody (green, 1:100 dilution) and Alexa Fluor 594-conjugated anti-goat IgG antibody (red, 1:100 dilution). Sections were also stained with DAPI to identify nuclear layers. Images were collected with a Zeiss LSM 510 laser-scanning confocal microscope with ×40/1.3 oil immersion objective (Neofluar oil). Colocalization of AE3 and CAXIV is indicated as merge and with yellow fluorescence. Scale bars = 25 μm. *C*: retinal lysate (Lys) from $ae3^{+/+}$ mice was immunoprecipitated with antibody directed against CAXIV. Samples were electrophoresed on 7.5% acrylamide gels, transferred to a PVDF membrane, and probed on with anti-AE3 antibody.

type ae3$^{+/+}$ and ae3$^{-/-}$ mice retinas displayed strong CAXIV expression (Fig. 7*A*). Confocal images showed extensive colocalization of AE3 and CAXIV in the inner retina, as observed in merged images (Fig. 7*B*, yellow). ae3$^{-/-}$ mice, or mice with a targeted disruption of the caXIV gene (caXIV$^{-/-}$) (39), were devoid of colocalization of AE3 and CAXIV, demonstrating specificity on the expression pattern of AE3 and CAXIV in the mouse retina (Fig. 7*B*). Anti-CAXIV antibody was able to precipitate AE3c from wild-type ae3$^{+/+}$ mouse retinal lysates (Fig. 7*C*). AE3 did not precipitate with the CAXIV antibody in lysates

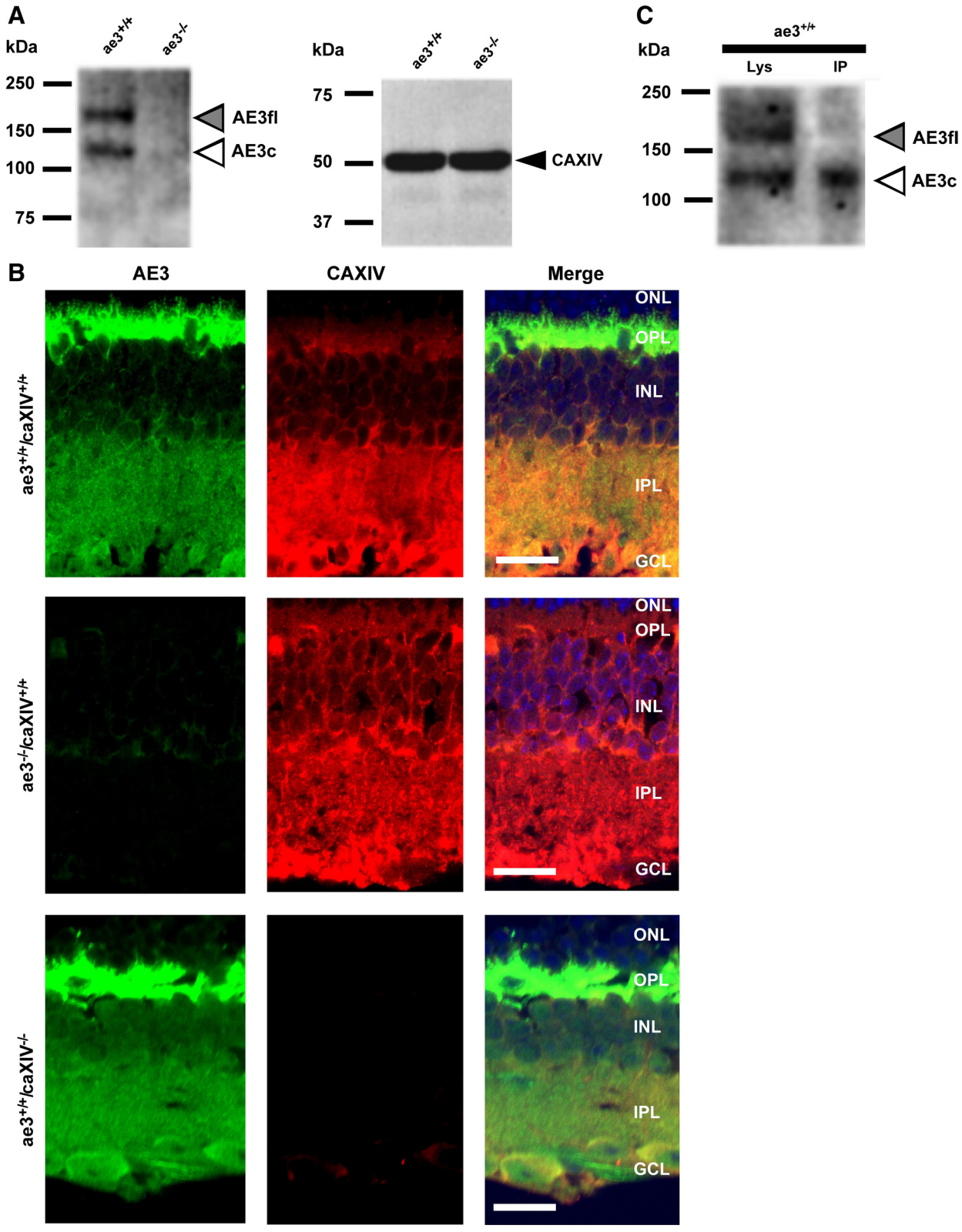

of ae3$^{-/-}$ mouse retina (not shown). From these immunoprecipitation experiments, we conclude that the CAXIV enzyme is physically associated with AE3 in mouse retina, more specifically in the inner retina.

Taken together, these experiments demonstrate that the AE3 Cl^-/HCO_3^- exchanger and the CAXIV plasma membrane-anchored carbonic anhydrase are functionally and physically coupled, forming a newly identified extracellular component of a HCO_3^- transport metabolon in excitable tissues.

DISCUSSION

Bicarbonate metabolism and transport are key elements of retinal, cardiac, and brain function. In the present study we have demonstrated a role played by the interaction of the AE3 Cl^-/HCO_3^- exchanger and the CAXIV enzyme in excitable tissues. CAXIV bound to and enhanced Cl^-/HCO_3^- exchange activity of AE3, establishing a physical and functional coupling. CAXIV maximizes HCO_3^- fluxes through AE3 in specialized cells of the CNS.

We have demonstrated that the expression of CAXIV, with catalytic site anchored to the extracellular surface, enhanced AE3-mediated Cl^-/HCO_3^- exchange activity by 120% in HEK293 cells expressing AE3fl and CAXIV. Cl^-/HCO_3^- exchange activity by AE3 was inhibited by ~75% with the potent membrane-permeant CA inhibitor ACTZ when AE3fl was coexpressed with CAXIV in HEK293 cells, suggesting that CAXIV catalytic activity is required for the increase of AE3 transport activity. However, we cannot exclude the possibility that ACTZ could have some degree of direct inhibitory effect on AE3.

In addition to the functional link between AE3 and CAXIV, we found that they form a physical complex in excitable tissues. Coimmunoprecipitation experiments demonstrated the structural association of AE3 and CAXIV when lysates of mouse brain and retinal tissue were immunoprecipitated with specific goat anti-CAXIV antibody, and the complex formed detected with rabbit anti-AE3 antibody.

Organization of proteins into a structural/functional metabolon will increase the flux of substrates through a linked metabolic pathway. Initial observations of carbonic anhydrase/bicarbonate transporter (CA/BT) interactions were made in the erythrocyte with AE1 and CAII (52). Several lines of evidence have shown that the two proteins associate (50, 51). Further studies revealed the nature of the CAII/AE1 interaction: *1*) pH dependence of CAII/AE1 interaction, suggesting requirement for structural electrostatic interactions (50), and *2*) functional involvement of the CAII/AE1 interaction, indicating that endogenous CAII is essential for efficient AE1 activity (44). The discovery of the CAII/AE1 physical/functional interaction led to studies of other members of the HCO_3^- transport superfamily, namely, AE2 and AE3 Cl^-/HCO_3^- exchangers (AE family) (44), NBC1 and NBC3 Na^+/HCO_3^- cotransporters (NBC family) (2, 11, 19, 32), and other BT members of the SLC26 family such as SLC26A3 (42), SLC26A6 (3), and SLC26A7 (22). AEs, NBC1 and NBC3, and SLC26A6 have been shown to form a physical/functional complex with CAII. CAII catalytic activity accelerates the rate of SLC26A3- and SLC26A7-mediated Cl^-/HCO_3^- exchange activity, but they do not require CAII binding for the acceleration (22, 42). Thus, the proximity of the freely diffusible CAII may suffice to facilitate bicarbonate transport. The bicarbonate transport metabolon extends beyond CAII. CAIV, which is GPI-linked to the extracellular surface, interacts with extracellular loop 4 of AE1 and NBC1 (2, 41). Furthermore, CAIX, which is anchored to the extracellular surface by a transmembrane segment, placing its highly active catalytic domain on the extracellular side of the plasma membrane, binds to AE2 Cl^-/HCO_3^- exchanger (22). In addition, the catalytic domain of CAIX binds SLC4 Cl^-/HCO_3^- exchangers and enhances transmembrane HCO_3^- flux mediated by AE1, AE2, and AE3 (22).

The driving force for the bicarbonate transport metabolon is the high concentration of HCO_3^- at the active site of the transporter, and the low concentration of HCO_3^- on the opposite side of the membrane. When a BT is associated with both a soluble CA (CAII), and a membrane linked (CAIV), or a single trans-membrane CA (CAIX and CAXIV), having the proteins so closely associated creates a microenvironment around the BT that allows for a tightly controlled bicarbonate concentration gradient. CAII, CAIV, CAIX, or CAXIV can generate the substrate for a BT, preventing depletion of HCO_3^- levels close to the transporter that could otherwise limit transport rate. On the trans-side of the membrane, the CA can consume the substrate passing through the BT, minimizing the concentration of HCO_3^- near the trans-surface of the transporter. In hippocampal neurons, the enhancement of AE3-mediated Cl^-/HCO_3^- exchange by surface CA (CAIV and CAXIV) was robust without cooperation of any intracellular CA activity, indicating a less dominant role of soluble cytosolic CA in the BT function in this case (46). Therefore, the AE3/CAXIV metabolon may have a greater role in sustaining CO_2 concentrations in neurons.

In the visual system, AE3 activity normally contributes to the regulation of $[Cl^-]$, pH_i, and cell volume. Working in concert with CAII and CAXIV, AE3 may contribute to the removal of CO_2 produced by photoreceptors. In addition, CAII and CAXIV, along with AE3c, could also be involved in tight regulation of horizontal retinal cells pH_i, increasing the effectiveness of the bicarbonate buffer system. Recently, functional defects in the ae3$^{-/-}$ mice were detected, as assessed by electroretinograms (ERGs) (1). In the ae3$^{-/-}$ mice, ERG a-wave and b-wave, which respectively represent photoreceptor and inner retina activity, were reduced, resulting in visual losses. In addition, a delayed but progressive phototransduction failure was also observed in ae3$^{-/-}$-null mice. Delayed onset of photoreceptor dysfunction could be attributable, in part, to prolonged Müller cell pathology as observed in retinal dystrophies (4). Functional abnormalities in ae3$^{-/-}$ mice retinas were accompanied by increased protein expression of CAII and CAXIV, and NBC1 Na^+/HCO_3^- cotransporter, suggesting compensation for the loss of AE3. The ability to maintain acid-base balance in the ae3$^{-/-}$ inner retina was dramatically compromised and was not fully compensated by other pH regulatory proteins. Anatomical pathological features and late onset cell death accompanied functional defects in ae3$^{-/-}$ mice retinas (1).

In the eye, CAXIV is predominantly expressed in retinal Müller glial cells, astrocytes, and RPE, spanning the entire thickness of the retina (24, 25). CAXIV distribution pattern is consistent with involvement in extracellular pH regulation and trans-retinal transport functions. An extracellular CA activity, most likely CAXIV, buffers the excess acidification in retina

under certain metabolic conditions by preventing increase in H^+ concentration (13).

A mouse deficient for caXIV (caXIV$^{-/-}$) has been recently described, with intriguing similarities to the phenotype of ae3$^{-/-}$ mice (39). Flash ERGs performed at 2, 7, and 10 mo of age showed that the rod/cone a-wave, b-wave, and cone b-wave were significantly reduced (up to 45%) in the caXIV$^{-/-}$ mice compared with its wild-type littermates (26). Thus, the phenotype was much milder than in the ae3$^{-/-}$-null mice, since transport by AE3 is still substantial without CAXIV (Fig. 1). Moreover, reductions in the dark-adapted response were not progressive between 2 and 10 mo, as previously observed for ae3$^{-/-}$ mice.

Additional information regarding cognitive capacities, seizure threshold, and sensitivity to seizure-inducing agents is required for the caXIV knockout animals. Double-knockout animals resulting from caXIV$^{-/-}$ and ae3$^{-/-}$ mating, if viable, might also bring additional information on the role of the AE3/CAXIV complex in the brain and other excitable tissues.

AE3fl is thought to participate in the removal of HCO_3^- from neurons, regulating pH_i (12, 15). A susceptibility locus for a common subtype of idiopathic generalized epilepsy (IGE) identified the chromosomal region 2q36 that includes S*LC4A3*, the gene encoding *AE3* (35). Later, a polymorphism within the coding sequence of *SLC4A3*, which carries the amino acid mutation Ala867Asp, was shown to be associated with IGE (36). To date, it remains unclear whether the 867Asp polymorphism itself functionally confers the risk for epileptic seizures. The Ala867Asp change has, however, recently been shown to reduce AE3 transport activity by about twofold, suggesting that loss of AE3 transport function is associated with elevation of epilepsy risk (49). Mice with a targeted disruption of the ae3 gene had a reduced seizure threshold, being more sensitive to seizure-inducing agents (12). Hence, these findings support the hypothesis that *AE3* is a susceptibility gene for epilepsy and is involved in the normal brain function.

Rapid shifts in interstitial pH accompanied neuronal discharge in the brain (6, 7). A key factor that modulates these changes is the pH buffer capacity of the extracellular fluid, a component closely regulated by extracellular CAIV and CAXIV function. As mentioned for AE3, CAXIV also contributes to the pH regulation of the brain, more specifically the hippocampus (39). Recently, CAIV and CAXIV were found to have important roles in the regulation of intracellular pH in the brain, by facilitating AE3-mediated Cl^-/HCO_3^- exchange in hippocampal neurons (46).

We conclude that AE3 and CAXIV act as a physical/functional complex in the brain, and that disruption of the interaction would impair CNS function. We suggest that the interaction of AE3 with extracellular carbonic anhydrase CAXIV is a new component of bicarbonate transport physiology. This study corroborates a general mechanism to modulate membrane transport activity: the interaction between peripheral enzymes and membrane transport proteins.

ACKNOWLEDGMENTS

We thank Anita L. Quon and Timothy Rubbelke for excellent technical assistance. We also thank Dr. Seth Alper (Beth Israel Deaconess Medical Center, Harvard Medical School, Boston, MA) for the AE3 (SA8) antibody. J. R. Casey is a Scientist of the Alberta Heritage Foundation for Medical Research (AHFMR, Canada). B. V. Alvarez is an Established Investigator of the Consejo Nacional de Investigaciones Científicas y Técnicas (CONICET, Argentina).

GRANTS

This work was supported by Canadian Institutes of Health Research Grants (CIHR, Canada) to J. R. Casey, Agencia Nacional de Promoción Científica Grant [PICT 2007 no. 01011, Fondo para la Investigación Científica y Tecnológica (FONCyT), Argentina] to B. V. Alvarez, and National Institutes of Health Grant DK40163 to W. S. Sly.

REFERENCES

1. **Alvarez BV, Gilmour GS, Mema SC, Martin BT, Shull GE, Casey JR, Sauve Y.** Blindness caused by deficiency in AE3 chloride/bicarbonate exchanger. *PLoS ONE* 2: e839, 2007.
2. **Alvarez BV, Loiselle FB, Supuran CT, Schwartz GJ, Casey JR.** Direct extracellular interaction between carbonic anhydrase IV and the human NBC1 sodium/bicarbonate co-transporter. *Biochemistry* 42: 12321–12329, 2003.
3. **Alvarez BV, Vilas GL, Casey JR.** Metabolon disruption: a mechanism that regulates bicarbonate transport. *EMBO J* 24: 2499–2511, 2005.
4. **Bringmann A, Pannicke T, Grosche J, Francke M, Wiedemann P, Skatchkov SN, Osborne NN, Reichenbach A.** Muller cells in the healthy and diseased retina. *Prog Retina Eye Res* 25: 397–424, 2006.
5. **Cordat E, Casey JR.** Bicarbonate transport in cell physiology and disease. *Biochem J* 417: 423–439, 2009.
6. **Chesler M.** Regulation and modulation of pH in the brain. *Physiol Rev* 83: 1183–1221, 2003.
7. **Chesler M, Kaila K.** Modulation of pH by neuronal activity. *Trends Neurosci* 15: 396–402, 1992.
8. **Chiappe de Cingolani GE, Ennis IL, Morgan PE, Alvarez BV, Casey JR, Camilion de Hurtado MC.** Involvement of AE3 isoform of Na^+-independent Cl^-/HCO_3^- exchanger in myocardial pH_i recovery from intracellular alkalization. *Life Sci* 78: 3018–3026, 2006.
9. **Ennis IL, Alvarez BV, Camilion de Hurtado MC, Cingolani HE.** Enalapril induces regression of cardiac hypertrophy and normalization of pH_i regulatory mechanisms. *Hypertension* 31: 961–967, 1998.
10. **Fabiato A, Fabiato F.** Effects of pH on the myofilaments and the sarcoplasmic reticulum of skinned cells from cardiac and skeletal muscles. *J Physiol* 276: 233–255, 1978.
11. **Gross E, Pushkin A, Abuladze N, Fedotoff O, Kurtz I.** Regulation of the sodium bicarbonate cotransporter kNBC1 function: role of Asp(986), Asp(988) and kNBC1-carbonic anhydrase II binding. *J Physiol* 544: 679–685, 2002.
12. **Hentschke M, Wiemann M, Hentschke S, Kurth I, Hermans-Borgmeyer I, Seidenbecher T, Jentsch TJ, Gal A, Hubner CA.** Mice with a targeted disruption of the Cl^-/HCO_3^- exchanger AE3 display a reduced seizure threshold. *Mol Cell Biol* 26: 182–191, 2006.
13. **Kniep EM, Roehlecke C, Ozkucur N, Steinberg A, Reber F, Knels L, Funk RH.** Inhibition of apoptosis and reduction of intracellular pH decrease in retinal neural cell cultures by a blocker of carbonic anhydrase. *Invest Ophthalmol Vis Sci* 47: 1185–1192, 2006.
14. **Kobayashi S, Morgans CW, Casey JR, Kopito RR.** AE3 Anion exchanger isoforms in the vertebrate retina: developmental regulation and differential expression in neurons and glia. *J Neurosci* 14: 6266–6279, 1994.
15. **Kopito RR, Lee BS, Simmons DM, Lindsey AE, Morgans CW, Schneider K.** Regulation of intracellular pH by a neuronal homolog of the erythrocyte anion exchanger. *Cell* 59: 927–937, 1989.
16. **Kramer BK, Smith TW, Kelly RA.** Endothelin and increased contractility in adult rat ventricular myocytes. Role of intracellular alkalosis induced by activation of the protein kinase C-dependent Na^+-H^+ exchanger. *Circ Res* 68: 269–279, 1991.
17. **Leem CH, Lagadic-Gossmann D, Vaughan-Jones RD.** Characterization of intracellular pH regulation in the guinea-pig ventricular myocyte. *J Physiol* 517: 159–180, 1999.
18. **Lindsey AE, Schneider K, Simmons DM, Baron R, Lee BS, Kopito RR.** Functional expression and subcellular localization of an anion exchanger from choroid plexus. *Proc Natl Acad Sci USA* 87: 5278–5282, 1990.
19. **Loiselle FB, Morgan PE, Alvarez BV, Casey JR.** Regulation of the human NBC3 Na^+/HCO_3^- cotransporter by carbonic anhydrase II and PKA. *Am J Physiol Cell Physiol* 286: C1423–C1433, 2004.

20. **Ma E, Haddad GG.** Expression and localization of Na^+/H^+ exchangers in rat central nervous system. *Neuroscience* 79: 591–603, 1997.
21. **McMurtrie HL, Cleary HJ, Alvarez BV, Loiselle FB, Sterling D, Morgan PE, Johnson DE, Casey JR.** The bicarbonate transport metabolon. *J Enzym Inhib Med Chem* 19: 231–236, 2004.
22. **Morgan PE, Pastorekova S, Stuart-Tilley AK, Alper SL, Casey JR.** Interactions of transmembrane carbonic anhydrase, CAIX, with bicarbonate transporters. *Am J Physiol Cell Physiol* 293: C738–C748, 2007.
23. **Morgan PE, Supuran CT, Casey JR.** Carbonic anhydrase inhibitors that directly inhibit anion transport by the human Cl^-/HCO_3^- exchanger, AE1. *Mol Membr Biol* 21: 423–433, 2004.
24. **Nagelhus EA, Mathiisen TM, Bateman AC, Haug FM, Ottersen OP, Grubb JH, Waheed A, Sly WS.** Carbonic anhydrase XIV is enriched in specific membrane domains of retinal pigment epithelium, Muller cells, and astrocytes. *Proc Natl Acad Sci USA* 102: 8030–8035, 2005.
25. **Ochrietor JD, Clamp MF, Moroz TP, Grubb JH, Shah GN, Waheed A, Sly WS, Linser PJ.** Carbonic anhydrase XIV identified as the membrane CA in mouse retina: strong expression in Muller cells and the RPE. *Exp Eye Res* 81: 492–500, 2005.
26. **Ogilvie JM, Ohlemiller KK, Shah GN, Ulmasov B, Becker TA, Waheed A, Hennig AK, Lukasiewicz PD, Sly WS.** Carbonic anhydrase XIV deficiency produces a functional defect in the retinal light response. *Proc Natl Acad Sci USA* 2007.
27. **Orchard CH, Kentish JC.** Effects of changes of pH on the contractile function of cardiac muscle. *Am J Physiol* 27: C967–C981, 1990.
28. **Parkkila S, Parkkila AK, Rajaniemi H, Shah GN, Grubb JH, Waheed A, Sly WS.** Expression of membrane-associated carbonic anhydrase XIV on neurons and axons in mouse and human brain. *Proc Natl Acad Sci USA* 98: 1918–1923, 2001.
29. **Pastorek J, Pastorekova S, Callebaut I, Mornon JP, Zelnik V, Opavsky R, Zat'ovicova M, Liao S, Portetelle D, Stanbridge EJ.** Cloning and characterization of MN, a human tumor-associated protein with a domain homologous to carbonic anhydrase and a putative helix-loop-helix DNA binding segment. *Oncogene* 9: 2877–2888, 1994.
30. **Pastorekova S, Parkkila S, Pastorek J, Supuran CT.** Carbonic anhydrases: current state of the art, therapeutic applications and future prospects. *J Enzym Inhib Med Chem* 19: 199–229, 2004.
31. **Perez NG, Alvarez BV, Camilion de Hurtado MC, Cingolani HE.** pH_i regulation in myocardium of the spontaneously hypertensive rat. Compensated enhanced activity of the Na^+-H^+ exchanger. *Circ Res* 77: 1192–1200, 1995.
32. **Pushkin A, Abuladze N, Gross E, Newman D, Tatishchev S, Lee I, Fedotoff O, Bondar G, Azimov R, Nguyen M, Kurtz I.** Molecular mechanism of kNBC1-carbonic anhydrase II interaction in proximal tubule cells. *J Physiol* 15: 55–65, 2004.
33. **Roos A, Boron WF.** Intracellular pH. *Physiol Rev* 61: 296–434, 1981.
34. **Ruetz S, Lindsey AE, Ward CL, Kopito RR.** Functional activation of plasma membrane anion exchangers occurs in a pre-Golgi compartment. *J Cell Biol* 121: 37–48, 1993.
35. **Sander T, Schulz H, Saar K, Gennaro E, Riggio MC, Bianchi A, Zara F, Luna D, Bulteau C, Kaminska A, Ville D, Cieuta C, Picard F, Prud'homme JF, Bate L, Sundquist A, Gardiner RM, Janssen GA, de Haan GJ, Kasteleijn-Nolst-Trenite DG.** Bader A, Lindhout D, Riess O, Wienker TF, Janz D, Reis A. Genome search for susceptibility loci of common idiopathic generalised epilepsies. *Hum Mol Genet* 9: 1465–1472, 2000.
36. **Sander T, Toliat MR, Heils A, Leschik G, Becker C, Ruschendorf F, Rohde K, Mundlos S, Nurnberg P.** Association of the 867Asp variant of the human anion exchanger 3 gene with common subtypes of idiopathic generalized epilepsy. *Epilepsy Res* 51: 249–255, 2002.
37. **Scheibe RJ, Gros G, Parkkila S, Waheed A, Grubb JH, Shah GN, Sly WS, Wetzel P.** Expression of membrane-bound carbonic anhydrases IV, IX, and XIV in the mouse heart. *J Histochem Cytochem* 54: 1379–1391, 2006.
38. **Schmitt BM, Berger UV, Douglas RM, Bevensee MO, Hediger MA, Haddad GG, Boron WF.** Na^+/HCO_3^- cotransporters in rat brain: expression in glia, neurons, and choroid plexus. *J Neurosci* 20: 6839–6848, 2000.
39. **Shah GN, Ulmasov B, Waheed A, Becker T, Makani S, Svichar N, Chesler M, Sly WS.** Carbonic anhydrase IV and XIV knockout mice: roles of the respective carbonic anhydrases in buffering the extracellular space in brain. *Proc Natl Acad Sci USA* 102: 16771–16776, 2005.
40. **Sperelakis N.** *Cell Physiology.* Academic Press, 1998, p. 1095.
41. **Sterling D, Alvarez BV, Casey JR.** The extracellular component of a transport metabolon. Extracellular loop 4 of the human AE1 Cl^-/HCO_3^- exchanger binds carbonic anhydrase IV. *J Biol Chem* 277: 25239–25246, 2002.
42. **Sterling D, Brown NJ, Supuran CT, Casey JR.** The functional and physical relationship between the DRA bicarbonate transporter and carbonic anhydrase II. *Am J Physiol Cell Physiol* 283: C1522–C1529, 2002.
43. **Sterling D, Casey JR.** Transport activity of AE3 chloride/bicarbonate anion-exchange proteins and their regulation by intracellular pH. *Biochem J* 344: 221–229, 1999.
44. **Sterling D, Reithmeier RA, Casey JR.** A transport metabolon. Functional interaction of carbonic anhydrase II and chloride/bicarbonate exchangers. *J Biol Chem* 276: 47886–47894, 2001.
45. **Su YR, Klanke CA, Houseal TW, Linn SC, Burk SE, Varvil TS, Otterud BE, Shull GE, Leppert MF, Menon AG.** Molecular cloning and physical and genetic mapping of the human anion exchanger isoform 3 (SLC2C) gene to chromosome 2q36. *Genomics* 22: 605–609, 1994.
46. **Svichar N, Waheed A, Sly WS, Hennings JC, Hubner CA, Chesler M.** Carbonic anhydrases CA4 and CA14 both enhance AE3-mediated Cl^--HCO_3^- exchange in hippocampal neurons. *J Neurosci* 29: 3252–3258, 2009.
47. **Tureci O, Sahin U, Vollmar E, Siemer S, Gottert E, Seitz G, Parkkila AK, Shah GN, Grubb JH, Pfreundschuh M, Sly WS.** Human carbonic anhydrase XII: cDNA cloning, expression, and chromosomal localization of a carbonic anhydrase gene that is overexpressed in some renal cell cancers. *Proc Natl Acad Sci USA* 95: 7608–7613, 1998.
48. **Vandenberg JI, Metcalfe JC, Grace AA.** Mechanisms of pHi recovery after global ischemia in the perfused heart. *Circ Res* 72: 993–1003, 1993.
49. **Vilas GL, Johnson DE, Freund P, Casey JR.** Characterization of an epilepsy-associated variant of the human Cl^-/HCO_3^- exchanger AE3. *Am J Physiol Cell Physiol* 297: C526–C536, 2009.
50. **Vince JW, Carlsson U, Reithmeier RA.** Localization of the Cl^-/HCO_3^- anion exchanger binding site to the amino-terminal region of carbonic anhydrase II. *Biochemistry* 39: 13344–13349, 2000.
51. **Vince JW, Reithmeier RA.** Identification of the carbonic anhydrase II binding site in the Cl^-/HCO_3^- anion exchanger AE1. *Biochemistry* 39: 5527–5533, 2000.
52. **Vince JW, Reithmeier RAF.** Carbonic anhydrase II binds to the carboxyl-terminus of human band 3, the erythrocyte Cl^-/HCO_3^- exchanger. *J Biol Chem* 273: 28430–28437, 1998.
53. **Vithana EN, Morgan P, Sundaresan P, Ebenezer ND, Tan DT, Mohamed MD, Anand S, Khine KO, Venkataraman D, Yong VH, Salto-Tellez M, Venkatraman A, Guo K, Hemadevi B, Srinivasan M, Prajna V, Khine M, Casey JR, Inglehearn CF, Aung T.** Mutations in sodium-borate cotransporter SLC4A11 cause recessive congenital hereditary endothelial dystrophy (CHED2). *Nat Genet* 38: 755–757, 2006.
54. **Yang Z, Alvarez BV, Chakarova C, Jiang L, Karan G, Frederick JM, Zhao Y, Sauve Y, Li X, Zrenner E, Wissinger B, Hollander AI, Katz B, Baehr W, Cremers FP, Casey JR, Bhattacharya SS, Zhang K.** Mutant carbonic anhydrase 4 impairs pH regulation and causes retinal photoreceptor degeneration. *Hum Mol Genet* 14: 255–265, 2005.
55. **Yannoukakos D, Stuart-Tilley A, Fernandez HA, Fey P, Duyk G, Alper SL.** Molecular cloning, expression and chromosomal localization of two isoforms of AE3 anion exchanger from human heart. *Circ Res* 75: 603–614, 1994.